BIOCHEMISTRY
including biophysical chemistry & molecular biology

Article

pubs.acs.org/biochemistry

Conservation and Diversity in the Primary Forward Photodynamics of Red/Green Cyanobacteriochromes

Sean M. Gottlieb,[†] Peter W. Kim,[†] Che-Wei Chang,[†] Samuel J. Hanke,[†] Randeep J. Hayer,[†] Nathan C. Rockwell,[‡] Shelley S. Martin,[‡] J. Clark Lagarias,[‡] and Delmar S. Larsen*,[†]

[†]Department of Chemistry and [‡]Department of Molecular and Cell Biology, University of California, Davis, One Shields Avenue, Davis, California 95616, United States

Supporting Information

ABSTRACT: Phytochromes are red/far-red photosensory proteins that detect the ratio of red to far-red light. Crucial to light regulation of plant developmental biology, phytochromes are also found in fungi, bacteria, and eukaryotic algae. In addition to phytochromes, cyanobacteria also can contain distantly related cyanobacteriochromes (CBCRs) that, like phytochromes, utilize the photoisomerization of a linear tetrapyrrole (bilin) chromophore to convert between two photostates with distinct spectral properties. CBCRs exhibit a wide range of photostates spanning the visible and even near-ultraviolet spectrum. In both phytochromes and CBCRs, biosynthesis initially yields a holoprotein with bilin in the 15*Z* configuration, and the 15*E* photoproduct can often revert to the 15*Z* photostate in the absence of light (dark reversion). One CBCR subfamily, red/green CBCRs, typically exhibits red-absorbing dark states and green-absorbing photoproducts. Dark reversion is extremely variable in red/green CBCRs with known examples ranging from seconds to days. One red/green CBCR, NpR6012g4 from *Nostoc punctiforme,* is also known to exhibit forward photoconversion that has an unusually high quantum yield at ∼40% compared to 10−20% for phytochromes and CBCRs from other subfamilies. In the current study, we use time-resolved pump-probe absorption spectroscopy with broadband detection and multicomponent global analysis to characterize forward photoconversion of seven additional red/green CBCRs from *N. punctiforme* on an ultrafast time scale. Our results reveal that red/green CBCRs exhibit a conserved pathway for primary forward photoconversion but that considerable diversity exists in their excited-state lifetimes, photochemical quantum yields, and primary photoproduct stabilities.

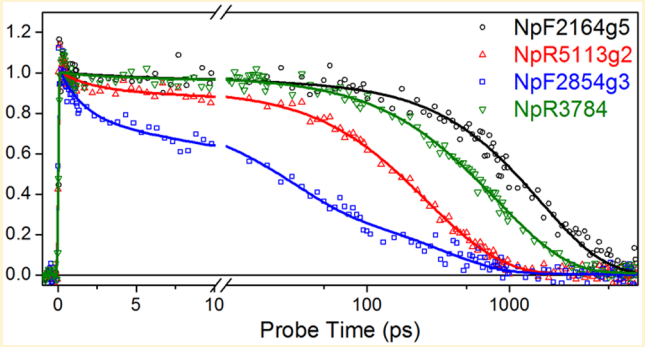

Increasing research efforts are being directed toward applying photoactive proteins to biological applications, such as genetically encoded fluorescent probes and light-regulated control of gene expression (optogenetics).[1−3] Such photosensory proteins exploit the excitation of bound chromophores to generate fluorescence or a biochemical signal that can then be transduced to the cell. Photoreceptors are thus important components in the growing biological "tool chest" of photoactive materials.[4−6] Although the mechanisms underlying photoinduced responses differ depending on the nature of the specific photoreceptor,[7] they typically originate from a small structural change in the chromophore that leads to large-scale structural rearrangements that modulate a biological "output" to interface with biological signal transduction pathways.[8]

Phytochrome photoreceptors use linear tetrapyrrole (bilin) chromophores to detect red (650−700 nm) and far-red (720−750 nm) light via reversible photoconversion between red- and far-red-absorbing forms (P_r and P_{fr}, respectively).[5,9] Phytochromes were initially discovered in plants, in which they regulate a wide range of light-induced responses,[10,11] and have subsequently been found in other photosynthetic organisms, including cyanobacteria, purple photosynthetic bacteria, and glaucophyte, charophyte, prasinophyte, cryptophyte, and heterokont algae.[5,12,13] Phytochromes have also been found in some nonphotosynthetic bacteria and filamentous fungi.[12,14,15] In such nonphotosynthetic organisms, phytochromes use biliverdin IXα as the chromophore, whereas plants and most cyanobacterial phytochromes typically utilize the more reduced phytochromobilin (PΦB) and phycocyanobilin (PCB) chromophores, respectively.[16] The primary photoreaction underlying phytochrome activity is an ultrafast (<1 ns) photoisomerization about the C15/C16 double bond of the bilin chromophore.[17−19] Widespread red/far-red phytochromes typically require a knotted photosensory core module of ≥500 amino acids for full, reversible photoconversion.[16,20] Cyanobacteria also can contain knotless phytochromes in which the red/far-red photocycle can still occur within a protein scaffold as small as ∼200 amino acids

Received: October 11, 2014
Revised: December 23, 2014
Published: December 29, 2014

DOI: 10.1021/bi5012755
Biochemistry 2015, 54, 1028−1042

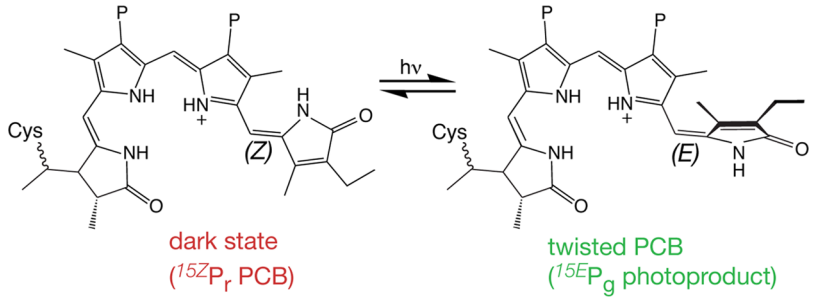

Figure 1. Photocycle of red/green CBCRs. $^{15Z}P_r$ is the dark stable state, and photoconversion results in trapping of a twisted 15*E* geometry in which the bilin D-ring is partially deconjugated to yield a blue-shifted $^{15E}P_g$ photoproduct.[39]

comprising a single bilin binding GAF domain.[21,22] Cyanobacteria also contain still smaller sensors termed cyanobacteriochromes (CBCRs), in which a slightly smaller GAF domain (~170 amino acids) is sufficient for PCB binding, covalent attachment, and full, reversible photoconversion.[23] Such CBCR domains are found in a wide range of cyanobacterial signaling proteins, and CBCRs have known roles in phototaxis, regulation of light-harvesting pigments, and biofilm formation.[23,24] Unlike phytochromes, known CBCRs do not sense far-red light, but instead exhibit an astonishing array of photocycles, affording cyanobacteria such as *Nostoc punctiforme* complete coverage of the visible and near-ultraviolet spectrum.[25,26]

Like phytochromes, CBCRs use photoisomerization about the C15/C16 double bond of the bilin chromophore as the primary photochemical event. De-excitation of the chromophore proceeds via a conical intersection with some fraction of the excited-state population undergoing photoisomerization to generate a primary photoproduct on an ultrafast time scale. The quantum yield for the formation of the primary photoproduct in phytochromes is typically 10−20%, but CBCRs can exhibit yields as high as 40%.[27] A number of different CBCR subfamilies have been identified by primary sequence and spectral properties. In one such subfamily, red/green CBCRs, the bilin chromophore adopts the 15*Z* configuration in the dark-adapted state of both the phytochrome (P_r) and red/green CBCR ($^{15Z}P_r$). In both cases, photoisomerization yields 15*E* bilin photoproducts, but the photoproducts have different spectral properties. Red/green CBCRs do not generate P_{fr} but rather generate a green-absorbing photoproduct ($^{15E}P_g$) (Figure 1).[6] Both P_{fr} and $^{15E}P_g$ can thermally revert to their respective red-absorbing, dark stable states in a process known as dark reversion. In red/green CBCRs, the rate of dark reversion is extremely variable with examples ranging from seconds to days; this allows CBCRs in this subfamily to act as color sensors or as broadband intensity sensors depending on the rate of dark reversion.[28]

Intermediates in the photocycle of red/green CBCRs have been examined in three isolated GAF domains to date. In AnPixJg2 from *Anabaena* (sp. PCC 7120), the only such protein for which there is a crystal structure,[29] intermediates have been studied on the nanosecond time scale.[30] NpR6012g4 and NpF2164g6 from *N. punctiforme* have been examined on an ultrafast time scale. NpR6012g4 exhibits an exceptionally high quantum yield (40%) for forward photoconversion from $^{15Z}P_r$ to $^{15E}P_g$ due to the formation of a productive ground-state intermediate (GSI) after de-excitation (second-chance initiation dynamics, SCID).[27] SCID is not present in NpF2164g6, demonstrating that there is diversity in the primary photophysical processes of closely related CBCRs.[31]

In the present study, we assess the extent of this diversity by examining forward photoconversion on an ultrafast time scale in seven additional red/green CBCRs from *N. punctiforme*. These seven proteins include an example that fails to form a photoproduct (NpF2164g5), an example with an atypically red-shifted photoproduct (NpR1597g4), and examples with a wide range of dark reversion rates. We also examined previously characterized NpF2164g6 to provide a direct comparison to previously acquired data. The results for these nine proteins were analyzed within a single global analysis framework and demonstrate broad conservation of the mechanism for primary forward photoconversion in photoactive red/green CBCRs. However, we find wide variation in the excited-state lifetimes, photochemical quantum yields, and stabilities of the Lumi-R_f primary photoproducts. Our studies thus reveal both conservation and diversity in a group of closely related photosensors undergoing the same primary photochemistry.

MATERIALS AND METHODS

CBCR Purification and Characterization. NpF2164g4, NpF2164g5, NpF2164g6, NpF2854g3, and NpAF142g2 were recombinantly expressed in *Escherichia coli* engineered to produce PCB,[32] and purification of GAF domains as intein−chitin binding domain (intein−CBD) fusions following a previously described procedure.[28] After lysis, ultracentrifugation, and binding to chitin resin (New England BioLabs) in accordance with the manufacturer's instructions, intein cleavage was initiated by addition of DTT to the column, followed by overnight incubation at 4 °C. Peak fractions were pooled and dialyzed against TKKG buffer (25 mM TES-KOH (pH 7.8), 100 mM KCl, 10% (v/v) glycerol) overnight prior to freezing in liquid nitrogen and storage at −80 °C. Absorbance spectra were acquired at 25 °C on a Cary 50 spectrophotometer. NpR1597g4, NpR5113g2, and NpR4776g3 were amplified from the previous intein−CBD construct using appropriate oligonucleotide primers and cloned into pET28-RcaE[33] for expression as His_6-tagged constructs. His-tagged proteins were expressed in *E. coli* strain C41[DE3] with plasmid pKT271 for PCB synthesis.[34,35] Protein was purified on Talon resin (Clontech) using an imidazole gradient (30−430 mM) with final dialysis into 20 mM sodium phosphate (pH 7.5), 50 mM NaCl, and 1 mM EDTA.

Transient Signals. The dispersed-probe transient absorption setup was constructed from an amplified Ti:sapphire laser system (Spectra Physics Spitfire Pro + Tsunami) operating at 1 kHz, which produced 2.25 mJ pulses of 800 nm fundamental output with a 40 fs (full width at half maximum) duration.[36]

DOI: 10.1021/bi5012755
Biochemistry 2015, 54, 1028−1042

The 800 nm fundamental pulse train from the amplifier was split into two paths. One path generated the dispersed white-light probe continuum (440−750 nm) by focusing the laser pulses into a slowly translating CaF_2 crystal. The second path was used to generate a tunable visible pulse from a home-built noncollinear optical parametric amplifier as an excitation/pump source, which was tuned (620−630 nm with 15−20 nm bandwidth) to be resonant with the visible absorption spectra of the samples for the transient absorption measurements (Figure 2 and Figure S1 in the Supporting Information (SI)).

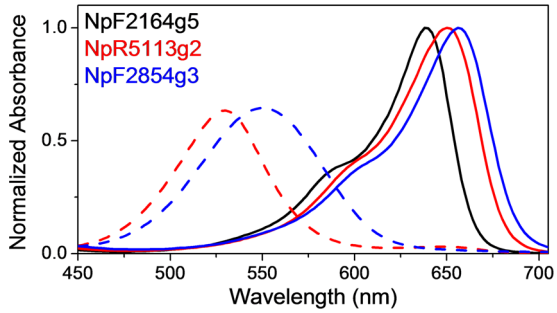

Figure 2. Ground-state absorption spectra for the $^{15Z}P_r$ (solid curves) and $^{15E}P_g$ (dashed curves) states of NpF2164g5 (black), NpR5113g2 (red), and NpF2854g3 (blue).[28] All spectra are scaled to the normalized $^{15Z}P_r$ absorption spectra.

The excitation pulse energies were set between 200 and 300 nJ depending on the sample. The pump beam was chopped at 500 Hz to generate difference spectra with respect to the nonpumped ground-state spectra. The probe beam was optically delayed with respect to the pump pulse by a computer-controlled linear motor stage (Newport IMS600LM), which allowed up to 8 ns temporal separation. Pump pulses were linearly polarized at 54.7° (magic angle) with respect to the probe pulses. The pump and probe pulse spot diameters at the sample were estimated using a moveable razor blade at 250−360 and 50 μm, respectively. The appreciably greater pump pulse area minimizes artifactual contributions to the signals due to varying spatial overlap between pump and probe beams and was confirmed by monitoring changes in signal amplitude and spectral shape while dithering the pump beam with respect to the probe beam.

The temporal resolution of the experiment was estimated to be 120 fs using the rise time of the excited-state absorption bands. Samples were flowed continuously (~30 mL/min) in a closed circuit to ensure fresh sample for each excitation pulse. Protein was continuously illuminated prior to entering a cuvette with ~5 mW of green (532 nm) continuous wave (CW) laser diode through a quartz window to maintain the sample in the P_r state during the ultrafast experiment. The path length of the quartz cuvette was 2 mm with the sample at an optical density of 0.3−0.4 (at that path length). All experiments were performed at room temperature (25 °C).

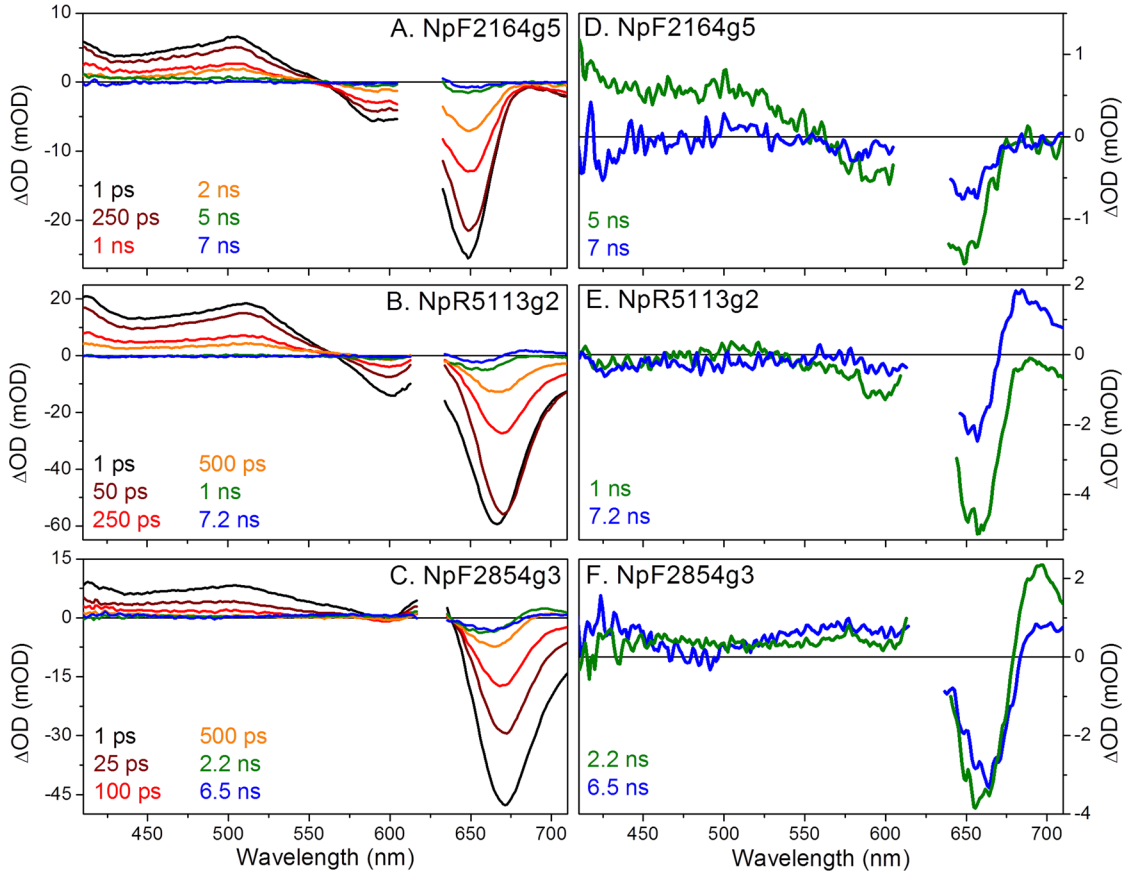

Figure 3. Transient absorption spectra for forward P_r* dynamics of (A) NpF2164g5, (B) NpR5113g2, and (C) NpF2854g3 at delay times specified in the graphs. All excited-state spectra exhibit similar spectral features but different kinetics (Figure 4). Transient absorption spectra at later delay times (as specified in the graphs) show photoproduct evolution more clearly for (D) NpF2164g5, (E) NpR5113g2, and (F) NpF2854g3.

DOI: 10.1021/bi5012755
Biochemistry 2015, 54, 1028−1042

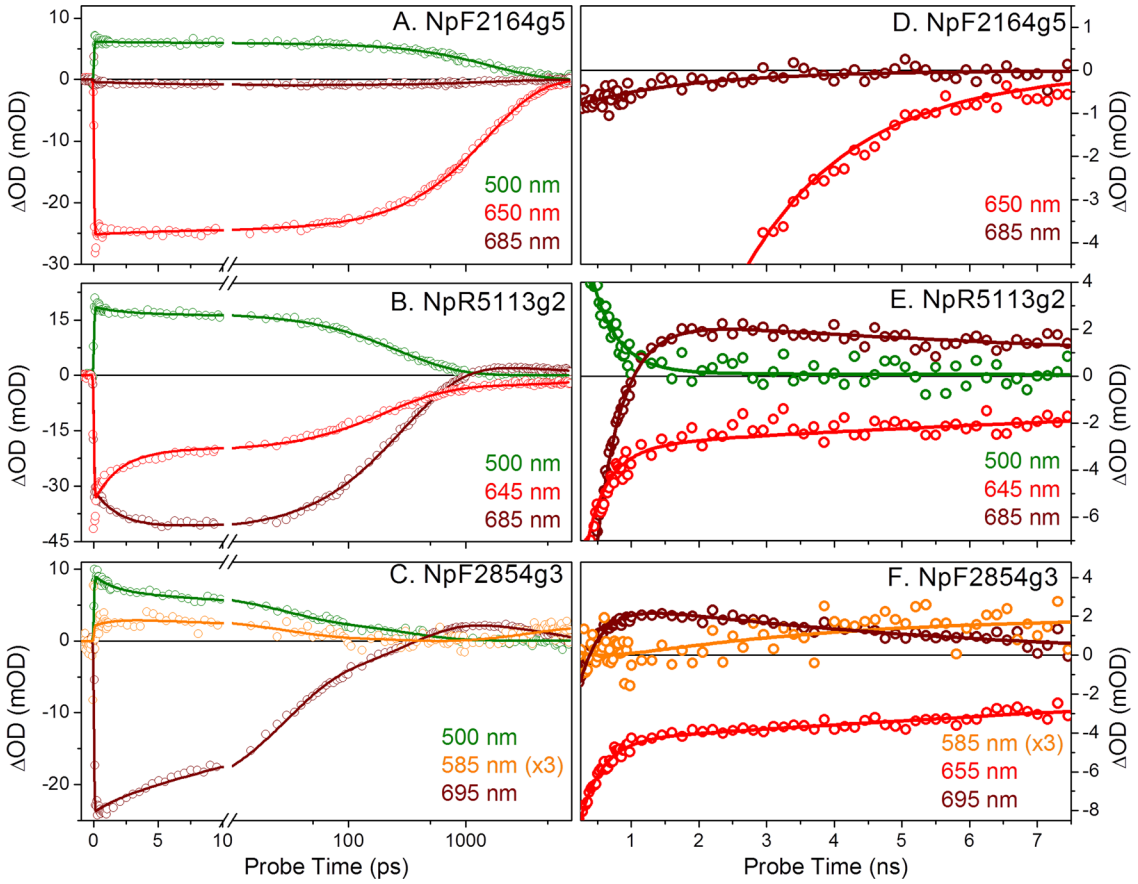

Figure 4. Kinetic traces for forward reaction P_r* dynamics of (A) NpF2164g5, (B) NpR5113g2, and (C) NpF2854g3 at the wavelengths indicated in the graphs. The wavelengths shown represent ESA (black circles), SE/Lumi-R_f (red circles), Meta-R_y (blue circles), and ground-state bleach (green circles). The solid curves are the fit by the respective target model (Figure 9). Kinetic traces at later delay times (1−8 ns) for (D) NpF2164g5, (E) NpR5113g2, and (F) NpF2854g3 detail the photoproduct and bleach band dynamics after excited-state decay. Kinetic traces are fit (solid lines) by their respective target models (Figure 9).

The 1 ms transient spectra were collected from the 1 kHz pulse train by shifting the probe pulse slightly before (∼1 ps) the pump pulse, which results in the collection of a transient spectrum initiated by the pump pulse from 1 ms earlier. To further facilitate this collection, the sample flow rate is typically slowed so that there is incomplete refreshing of new sample within the excitation laser volume in the flow cell. Under normal flow conditions, this pre-time zero signal (1 ms spectrum) is negligible. Subsequent "harmonic" dynamics (e.g., 4 ms) are not a major factor in these spectra because the flow rate has completely refreshed (within the excitation volume) on this time scale.

RESULTS

CBCR Samples. We measured forward dynamics for seven red/green CBCRs previously examined only on a static time scale: NpR1597g4, NpF2164g5, NpF2164g4, NpR4776g3, NpR5113g2, NpAF142g2, and NpF2854g3. We also collected data under identical conditions for previously characterized NpF2164g6,[31] allowing for comparison to these proteins and to the well-characterized red/green CBCR NpR6012g4.[27,31,37] Thus, ultrafast data are now available for a total of nine red/green CBCRs from *N. punctiforme* that are assigned to three classes on the basis of the yield and stability of the photoproduct on this time scale (<10 ns). Three CBCR domains (NpF2164g5, NpR5113g2, and NpF2854g3) are presented in detail here, whereas the others are presented in the SI. Normalized static absorption spectra for NpF2164g5, NpR5113g2, and NpF2854g3 in the $^{15Z}P_r$ dark state are contrasted in Figure 2 (solid black, red, and blue curves, respectively). The $^{15Z}P_r$ absorption bands (solid lines) of all three CBCR samples are qualitatively similar with a shoulder near 600 nm. Such shoulders have been interpreted as vibronic features in other biliproteins.[38] However, such shoulders can also arise due to the presence of blue-shifted side populations, and such blue-shifted species are indeed the majority population in known NpR6012g4 variants generated by site-directed mutagenesis.[39] NpF2164g5 fails to generate the $^{15E}P_g$ photoproduct,[28] but the photoproducts formed by NpR5113g2 and NpF2854g3 are similar to each other (Figure 2).

Transient Absorption Signals. Forward reaction dynamics of red/green CBCRs begin with the initial formation of excited-state $^{15Z}P_r$* followed by formation of the primary Lumi-R_f photoproduct and the subsequent formation of a Meta-R_y intermediate.[30,40] Depending on how fast these processes occur, it is possible that Meta-R_y formation could occur during the accessible time frame of this study (0−10 ns). Transient absorption (TA) spectra are shown for NpF2164g5, NpR5113g2, and NpF2854g3 at selected delay times in Figure 3 with corresponding kinetic traces at selected probe wavelengths in Figure 4. Transient signals for other CBCRs are presented in the SI (Figures S2−S6). The TA signals are a superposition of four overlapping signals: (1) a negative bleach

DOI: 10.1021/bi5012755
Biochemistry 2015, 54, 1028−1042

signal (ground-state bleach, GSB) caused by the loss of ground-state absorption (GSA), (2) a negative stimulated emission (SE) signal caused by photostimulated decay of the excited state, (3) positive excited-state absorption (ESA) caused by $S_1 \rightarrow S_n$ transitions from the first excited state (here, P_r*) to higher levels, and (4) positive photoproduct absorption caused by the appearance of ground-state photoproduct species (e.g., Lumi-R_f and Meta-R_y in the samples discussed here). Visual inspection of these signals allowed us to identify three categories:

1. Class I domains (NpR1597g4 and NpF2164g5) are no- or low-yielding samples. These proteins exhibit only excited-state P_r* signals with no resolvable photoproduct signals. Both samples exhibit long excited-state kinetics (apparent relaxation time τ = ~1 ns). This class of red/green CBCR domain is represented here by NpF2164g5, which does not produce the $^{15E}P_g$ state and has a high fluorescence quantum yield.[28] NpR1597g4 undergoes photoconversion upon continuous illumination despite our inability to detect Lumi-R_f on this time scale. We estimate a low quantum yield (Φ < 2%) for primary isomerization of NpR1597g4.

2. Class II domains (NpR5113g2, NpF2164g6, and NpR6012g4) exhibit both excited-state P_r* and Lumi-R_f signals with no apparent evolution of Lumi-R_f on an ultrafast time scale. This class of domains includes previously characterized NpR6012g4 and NpF2164g6 and is represented here by NpR5113g2.

3. Class III domains (NpAF142g2, NpR4776g3, NpF2854g3, and NpF2164g4) generate excited-state P_r*, Lumi-R_f, and Meta-R_y populations within the ultrafast time scale. Meta-R_y is formed after Lumi-R_f and exhibits broad blue-shifted absorption. It is spectrally analogous to the $R2_{610}$ intermediate resolved ~1 μs after photoexcitation of AnPixJg2 by Fukushima et al.[30] Class III CBCRs exhibit Lumi-R_f decay that is faster than that of class II CBCRs. This class is represented by NpF2854g3.

NpF2164g5, NpR5113g2, and NpF2854g3 exhibit similar excited-state P_r* spectra (Figure 3) with a broad ESA band from 410 to 550 nm (peaking at ~500 nm) and a broad negative region from 640 to 670 nm that is a mixture of bleach and SE bands. Given the known heterogeneity of NpR6012g4 and NpF2164g6,[31,37] the absence of isosbestic points in the TA signals (Figure 3 and Figure S4 in the SI) is not surprising. However, the signals in the spectral window from 580 to 630 nm (referred to as the "crossover region"), where the ESA and GSB overlap, maintain a near-zero amplitude throughout the primary photodynamics. The wavelength at which this point occurs varies; for example, this point is observed at ~558 nm for NpF2164g5, ~567 nm for NpR5113g2, and ~585 nm for NpF2854g3 (Figure 3). The crossover region is negative for NpF2164g5 and NpR5113g2 but positive for NpF2854g3 (Figure 3). This region is sensitive to small spectral shifts and/or to the dynamics of new populations, as demonstrated in the analysis of the forward dynamics of NpR6012g4.[37] A similar crossover region was useful in resolving underlying heterogeneity of the red/far red photoswitching canonical phytochrome Cph1 in excitation-dependent and temperature-dependent dynamics[41,42] and has been seen in other phytochromes.[43,44]

The ESA region (450−500 nm) provides a window for examining the decay kinetics of excited-state P_r* because this region suffers from the least overlap with GSB, SE, and photoproduct absorption. Inactive NpF2164g5 exhibits slow excited-state dynamics with an apparent half-life of ~1 ns (Figure 4A) and with no photoproduct formation at longer time points (Figure 4D). Excited-state decay was much faster in NpR5113g2 and NpF2854g3 (approximately 162 and 22 ps for NpR5113g2 and NpF2854g3, Figure 4B and C, respectively) but was obviously multiphasic. In NpR5113g2, an initial negative amplitude at 645 and 685 nm (Figure 4B) arises due to bleach and/or SE. Positive absorption at 685 nm after 1 ns reflects the formation of primary photoproduct Lumi-R_f, which persists for the duration of the experiment with ≤25% decay (Figure 4E). In NpF2854g3, an initial negative amplitude at 695 nm again arises from GSB and/or SE with clear formation of Lumi-R_f by 0.5 ns (Figure 4C). The subsequent decay of Lumi-R_f is much faster with ~75% of the maximal Lumi-R_f signal lost by 7.5 ns (Figure 4F). Initial positive signals at 585 nm for NpF2854g3 arise due to ESA because they decay along with the ESA signal at 500 nm (Figure 4C). However, a positive signal at 585 nm is regained at later time points (Figure 4F), correlating with the decay of Lumi-R_f and demonstrating rapid formation of Meta-R_y in this protein.

No positive Lumi-R_f signals are resolved in the class I protein NpF2164g5 (Figure 4A and D, red circles) indicating negligible Φ_{Lumi}. This is consistent with the known failure of NpF2164g5 to generate $^{15E}P_g$ under continuous red-light illumination.[28] A similar result was obtained with the other class I CBCR, NpR1597g4 (Figure S2 in the SI). For the Class II protein NpR5113g2, TA spectra at later time points show decay of ground-state bleach and formation of Lumi-R_f after 1 ns without formation of Meta-R_y (Figure 3E). The 7.5 ns spectrum of the class II CBCR NpR5113g2 (Figure 5B, cyan curve) shows a newly formed absorption band peaking near

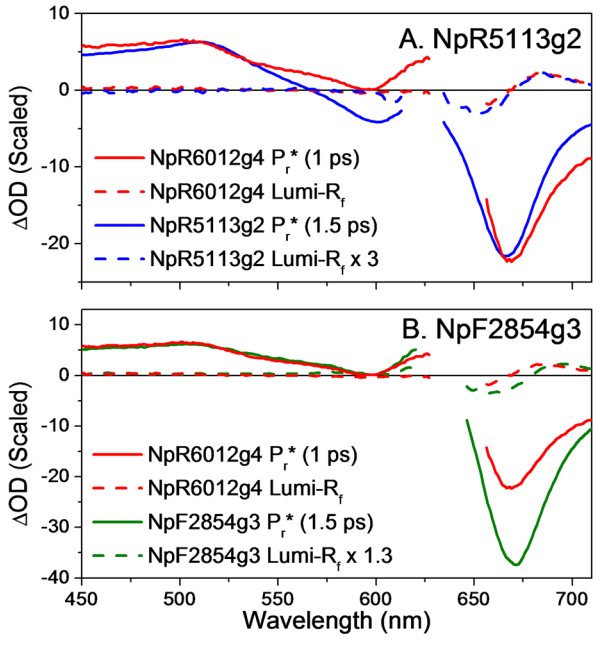

Figure 5. Excited-state transient spectra (solid curves) and Lumi-R_f (dashed curves) normalized at 500 nm. (A) The scaled Lumi-R_f spectrum for NpR5113g2 (blue dashed curve) is further scaled 3-fold to match the amplitude of the NpR6012g4 Lumi-R_f spectrum (red dashed curve). (B) The Lumi-R_f spectrum for Np2854g3 (green dashed curve) is scaled by 1.3-fold to match the equivalent amplitude of the NpR6012g4 Lumi-R_f spectrum (red dashed curve). Both comparisons indicate a greater Lumi-R_f quantum yield in NpR6012g4, assuming comparable extinction coefficients.

DOI: 10.1021/bi5012755
Biochemistry 2015, 54, 1028−1042

685 nm and a negative bleach band peaking at 660 nm, which are features consistent with the depletion of the starting $^{15Z}P_r$ ground state and formation of Lumi-R_f.[37,42−47] Similar results were obtained for NpF2164g6 (Figure S3 in the SI) and in previous analysis of NpR6012g4.[27,31] For the latter two proteins, Lumi-R_f decay was not observed on the ultrafast time scale. A modest Lumi-R_f decay was observed in NpR5113g2 at later time points and was accompanied by further decay of the bleach band (Figure 4E). This result could indicate that the Lumi-R_f population in NpR5113g2 can return to the $^{15Z}P_r$ ground state, implying a nonunity quantum yield for Meta-R_y formation. Alternately, it could indicate that Meta-R_y formation in NpR5113g2 proceeds via a red-absorbing intermediate in NpR5113g2 that cannot be resolved from the starting species on this time scale. Characterization of forward photoconversion in NpR5113g2 at later time points to monitor Meta-R_y formation will be required to resolve this question.

The TA spectra for class III protein NpF2854g3 show clear decay of Lumi-R_f absorption after 2.2 ns with the appearance of Meta-R_y absorption at 525−600 nm and little change in GSB (Figure 3F). This is consistent with the formation of Meta-R_y from Lumi-R_f rather than regeneration of $^{15Z}P_r$. Similar results were obtained for the other class III proteins in this study. In NpAF142g2 (Figure S4 in the SI), there is substantial Meta-R_y formation and loss of Lumi-R_f. In NpR4776g3 (Figure S5 in the SI) and NpF2164g4 (Figure S6 in the SI), loss of Lumi-R_f is less pronounced for the amount of Meta-R_y formation observed, perhaps indicating slight differences in the Meta-R_y extinction coefficient or stability. In all class III cases, slight changes in GSB are observed at late time points due to spectral overlap of negative GSB signals with positive Meta-R_y signals.

Estimated Quantum Yield. The quantum yield for generating Lumi-R_f ($\Phi_{Lumi\text{-}Rf}$) is an important parameter in characterizing the photodynamics of CBCR systems and provides an important constraint for model-based target analysis (see below), but its rigorous determination can prove challenging. The amount of the initially excited P_r* population can be compared to the maximum observed amplitude of the Lumi-R_f population. This approach unfortunately requires clean bleach wavelengths that are free of overlapping ESA, SE, and Lumi-R_f bands in the TA signals, a situation that does not pertain to the red/green CBCR signals shown here. We therefore used an indirect "reference approach" by comparing the TA signals to those measured with NpR6012g4. NpR6012g4's $\Phi_{Lumi\text{-}Rf}$ value was estimated at 32% using cyanobacterial phytochrome Cph1 as a reference[42,48] and was then directly measured to be 40% using multipulse pump-dump-probe (PDP) experiments.[37] Thus, NpR6012g4 provides a known reference value in a closely related system. However, this approach can still lead to systematic error in the current data set; it assumes that Lumi-R_f decay is much slower than Lumi-R_f formation, such that the maximum observed Lumi-R_f amplitude is the maximum that can be formed. Class III cases in which Lumi-R_f can decay on the ultrafast time scale may not meet this condition; thus, the values derived from this analysis may underestimate $\Phi_{Lumi\text{-}Rf}$ for such proteins. No attempt was made to estimate $\Phi_{Lumi\text{-}Rf}$ values for class I proteins, in which Lumi-R_f formation was not detected.

To use this indirect approach, we first scaled the initial amplitude of the ESA band at ∼500 nm for each protein in this study to that of NpR6012g4 (Figure 5 and Figure S7 in the SI). The ESA band in this region arises almost exclusively from excited-state transitions with little effect from GSB or photoproduct formation. Such ESA bands are generally viewed as a broad, featureless continuum, so protein-specific effects on the extinction coefficient for this band are less likely to be significant than for others in this analysis. We then scaled the time point having maximal Lumi-R_f amplitude for each protein to the Lumi-R_f spectrum of NpR6012g4 using the factor required for scaling the ESA band of that protein. Assuming the Lumi-R_f extinction coefficients are also comparable between the CBCRs, $\Phi_{Lumi\text{-}Rf}$ values for each protein can then be estimated by comparison with the Lumi-R_f amplitude of the NpR6012g4 reference. $^{15Z}P_r$ extinction coefficients for the proteins in this study vary by <30%;[28] thus, we anticipate similar variation in the Lumi-R_f extinction coefficients.

For NpR5113g2, the scaled Lumi-R_f spectrum is 3-fold lower than the NpR6012g4 Lumi-R_f amplitude (Figure 5A, blue and red dash curves, respectively), indicating that $\Phi_{Lumi\text{-}Rf}$ is approximately one-third of 40%, or ∼13%. Similarly, for NpF2854g3, the Lumi-R_f spectrum is scaled by a factor of 1.3 to match the NpR6012g4 Lumi-R_f amplitude (Figure 5B, green and red dash curves, respectively), indicating a $\Phi_{Lumi\text{-}Rf}$ value of ∼31% (40% divided by 1.3) for NpF2854g3. The same method was used to estimate the $\Phi_{Lumi\text{-}Rf}$ values for the other CBCRs, which ranged from 11 to 29% (Table 1 and Figure S7 in the SI). Several cases exhibit $\Phi_{Lumi\text{-}Rf}$ values that are much higher than those observed for cyanobacterial phytochromes (10−20%), indicating that the high $\Phi_{Lumi\text{-}Rf}$ values observed for NpR6012g4 and NpF2164g6 are not unique.[27,31] Estimated $\Phi_{Lumi\text{-}Rf}$ values were then used as constraints in target analysis.

Table 1. Quantum Yield Estimates[a]

sample	class	P_r absorption peak	P_g absorption peak	$\Phi_{Lumi\text{-}Rf}$
NpAF142g2	III	650 nm	534 nm	0.3
NpR1597g4	I	638 nm	574 nm	∼0.04
NpF2164g4	III	646 nm	532 nm	0.13
NpF2164g5	I	638 nm		
NpF2164g6	II	649 nm	551 nm	0.3
NpF2854g3	III	656 nm	550 nm	0.36
NpF4776g3	III	656 nm	560 nm	0.18
NpR5113g2	II	650 nm	530 nm	0.17
NpR6012g4	II	651 nm	540 nm	0.40

[a]Excited-state transient spectra were normalized at the initial amplitude of the ESA band at 500 nm. The magnitude of the final scaled Lumi-R_f spectrum of the samples studied after this normalization was then rescaled to match that of NpR6012g4. Assuming the Lumi-R_f populations exhibit comparable extinction coefficients (including the ESA and bleach bands), the $\Phi_{Lumi\text{-}Rf}$ value for each CBCR was then estimated from the scaling factor using the known $\Phi_{Lumi\text{-}Rf}$ value of NpR6012g4.[27]

Global Analysis. The TA signals for all proteins were analyzed using a multicompartment global analysis formalism[49,50] that decomposes the data with an underlying target model into time-dependent populations (i.e., concentration profiles) with time-independent spectra. This is accomplished by fitting the data with numerical solutions of linear first-order differential equations describing the postulated target model (eq 1).

$$\frac{dn_i}{dt} = A_i I(t) + \sum_{i,j} K_{ij} n_i \quad (1)$$

In eq 1, n_i represents the ith microscopic population of interest, A_i is the initial occupancy of the ith excited state, $I(t)$ is the

DOI: 10.1021/bi5012755
Biochemistry 2015, 54, 1028−1042

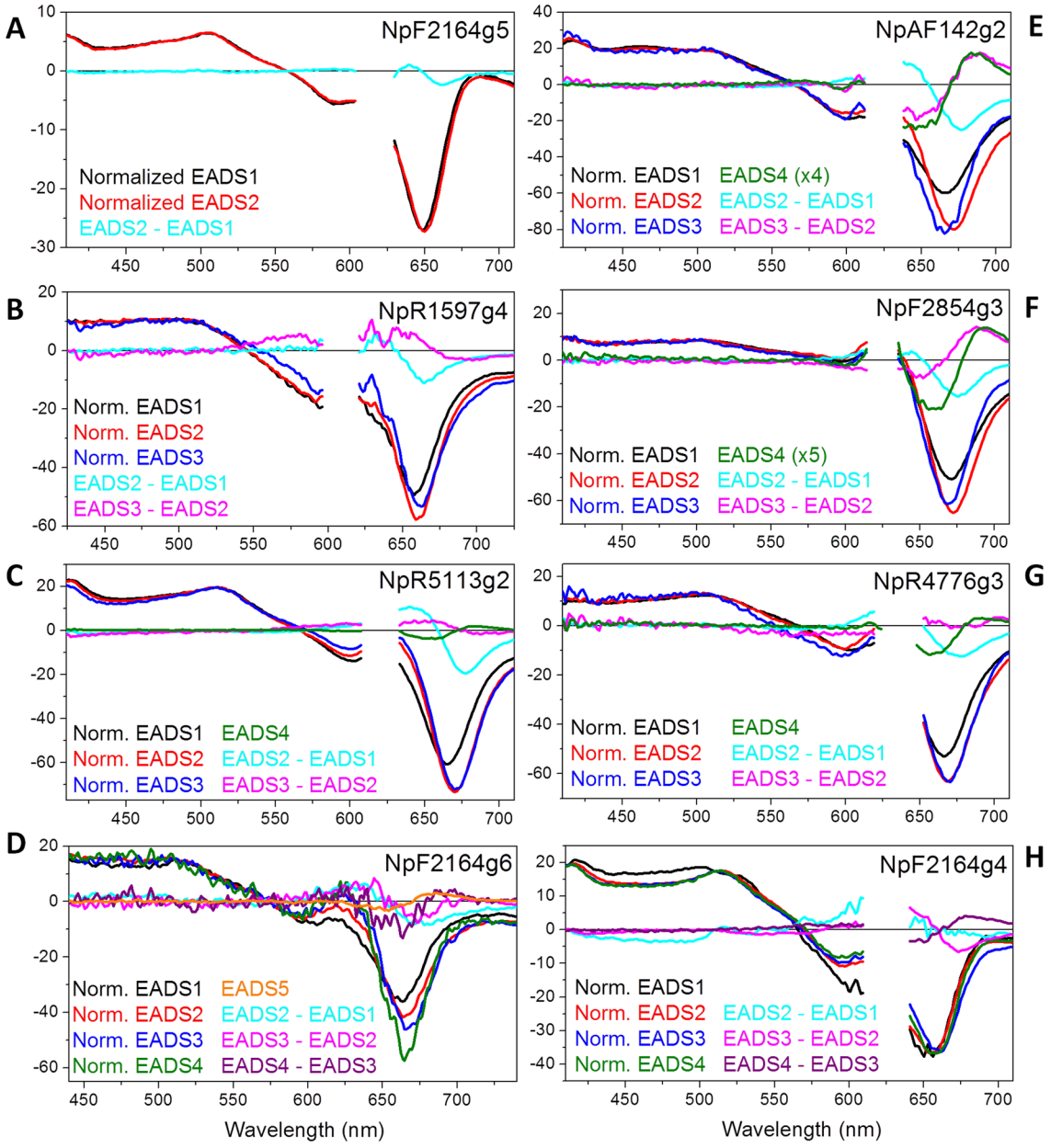

Figure 6. Decomposition of the EADS for each sample studied. Initial fast relaxation observed in many of the samples is characterized by a red-shift of the SE band (cyan curves) and does not result in the evolution of photoproduct. Spectra of the three CBCRs presented in the body of the manuscript are highlighted in yellow.

pump pulse temporal envelope, and K_{ij} are the rate constants describing the exponential flow from the *i*th population into the *j*th population. If the underlying target model accurately describes the dynamics, the extracted spectra from the analysis are termed species-associated difference spectra (SADS) and represent the true difference spectra of the constituent populations. If the model inaccurately describes the dynamics, the resulting spectra are linear combinations of the underlying SADS.[27,37,49,50] One common model used in the analysis of TA data is the sequential model, which generates evolution-associated difference spectra (EADS) from the global analysis. In systems with more complex dynamics, these spectra will also be linear combinations of SADS.

Accurate description of heterogeneous CBCR systems requires more sophisticated target analysis.[37,49−51] For all of the data sets, we began global analysis by fitting the data to a simple sequential model (Figure S8 in the SI). The EADS resulting from the sequential model can be used to extract useful information in CBCR systems, such as separating the time scales of Lumi-R_f formation from multiexponential excited-state dynamics,[37,51] and supply important *a priori* constraints on population flow for target model construction. The sequential EADS analyses of all of the CBCRs in this study are presented in Figure S9 in the SI. To help in decomposing the sequential EADS into viable SADS and facilitating target model construction, we evaluated the difference spectra between successive EADS (Figure 6). The class I NpF2164g5 TA signals are adequately described by two EADS (Figure 6A). The difference spectrum between these EADS exhibited a small positive peak at ~640 nm, matching the peak absorption of the $^{15Z}P_r$ ground state, and a small negative peak at ~660 nm, close to the reported fluorescence emission maximum of 655 nm.[28]

DOI: 10.1021/bi5012755
Biochemistry 2015, 54, 1028−1042

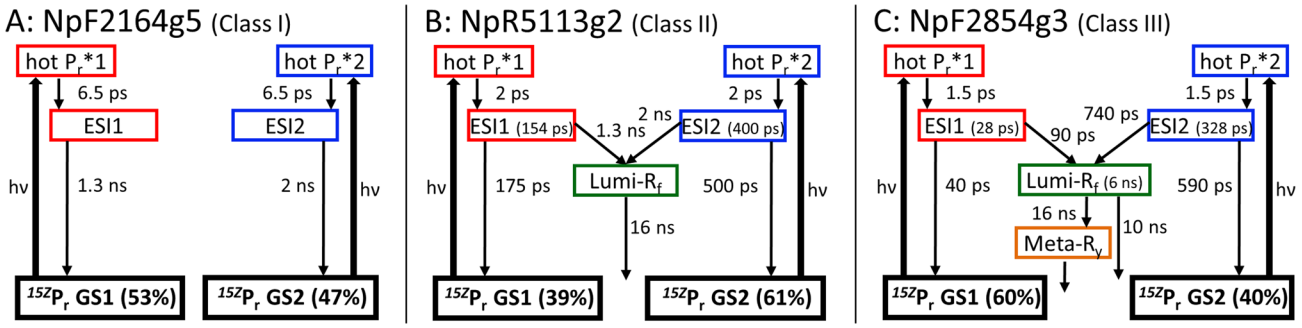

Figure 7. Target models for (A) NpF2164g5, (B) NpR5113g2, and (C) NpF2854g3. Population colors correspond to the concentration profiles in Figure 4. The majority of the samples require only two P_r ground-state populations to fit the data. Time constants and ground-state occupancy levels for these models can be found in Table 2.

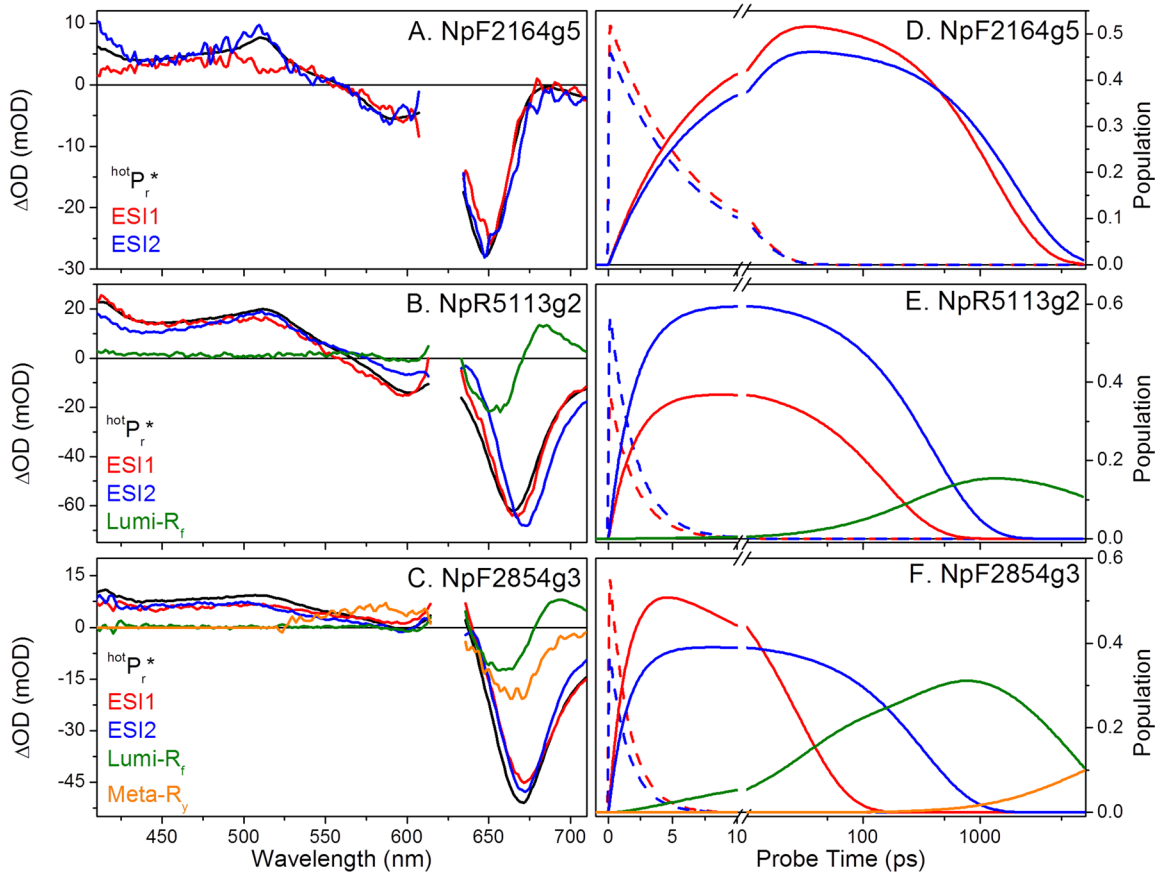

Figure 8. Global target analysis results for forward reactions with two ground-state populations. SADS based on the target models in Figure 7 are shown for (A) NpF2164g5, (B) NpR5113g2, and (C) NpF2854g3. Concentration profiles for each spectral species over time are shown for (D) NpF2164g5, (E) NpR5113g2, and (F) NpF2854g3. Curves for hot populations are dashed. Overall photoproduct quantum yields can be found in Table 1.

This analysis is consistent with a photochemically inactive protein exhibiting relaxation of the P_r* excited state to yield a small Stokes shift. NpR1597g4 exhibited further evolution with a final phase having a positive amplitude in the vicinity of the Meta-R_y band observed in other red/green CBCRs (Figure 6B). This small signal is likely to arise from a productive population given the discrepancy between the absence of Lumi-R_f signals in NpR1597g4 and its known photoconversion under static conditions.[28]

Sequential EADS analysis of class II CBCR NpR5113g2 was more complex with a total of four EADS (Figure 6C) required. Excited-state features persist in EADS3, but the EADS3−EADS2 difference spectrum resembled an inverted EADS4, indicative of product formation at the earlier phase in addition to later at EADS4. NpR5113g2 is thus heterogeneous with Lumi-R_f formation occurring on at least two time scales. A similarly complex evolution was observed for NpF2164g6, the other class II protein examined in this study (Figure 6D). The class III CBCRs are distinguished by rapid formation of Meta-R_y from Lumi-R_f as reflected in their sequential EADS: all five such proteins have four EADS with the last reflecting Meta-R_y formation (Figure 6E−H). The features observed in the sequential EADS for these CBCRs were then used to construct a general multicompartment target model encompassing the

DOI: 10.1021/bi5012755
Biochemistry 2015, 54, 1028−1042

Table 2. Parameters for the Formation of Lumi-R_f

						ESI1 (ps)			ESI2 (ps)			ESI3 (ps)
sample	class	GS1 (%)	GS2 (%)	GS3 (%)	$^{Hot}P_r$* (ps)	τ_{app}	→ GS	→ Lumi-R_f	τ_{app}	→ GS	→ Lumi-R_f	→ GS
NpAF142g2	III	55	45		1.5	33	45	130	261	400	750	
NpR1597g4	I	100			5.7	950	1100	2600				
NpF2164g4	III	41	59		1.2	20	22	235	483	575	3010	
NpF2164g5	I	53	47		6.5	1300	1300		2000	2000		
NpF2164g6	II	35	35	30	0.3	44.2	138	65	330	400	2000	4.3
NpF2854g3	III	60	40		1.5	27.7	40	90	330	588	740	
NpF4776g3	III	61	39		0.7	12.9	13	1500	120	225	275	
NpR5113g2	II	39	61		2	154	175	1275	400	500	2000	
NpR6012g4	II	33	23	44		55	204	75	330	492	1000	5

observed variation among proteins (Figure S10 in the SI). This model includes a heterogeneous ground state with up to three coexisting subpopulations (i.e., inhomogeneity), two of which can be productive. The justification for such a model (versus branched or sequential models) has been discussed in detail in previous analysis of other CBCRs.[37,51] Initial excited-state relaxation yields one to three excited-state intermediates (ESI1−ESI3), which partition between Lumi-R_f and the starting ground state upon de-excitation. Lumi-R_f can itself evolve to Meta-R_y. To model the loss of Lumi-R_f and GSB at late time points in NpR5113g2, we allowed Lumi-R_f to decay back to the starting ground state in the absence of any other evidence for a hypothetical Meta-R_r in this protein. The general target model was then customized for each of the proteins in this study.

The target models constructed for NpF2164g5, NpR5113g2, and NpF2854g3 are presented in Figure 7, and the corresponding SADS and concentration profiles are presented in Figure 8. Equivalent information is presented for the remaining samples in Figures S11 and S12 of the SI with parameters presented in Tables 2 and 3. The accuracy of these

Table 3. Parameters for the Evolution of Primary Photoproducts

		Lumi-R_f			
sample	class	Φ_{Lumi}	τ (ns)	→ GS (ns)	→ Meta-R_y (ns)
NpAF142g2	III	0.3	∼11	slow	11
NpR1597g4	I	0.04			
NpF2164g4	III	0.13	7.92	800	8
NpF2164g5	I				
NpF2164g6	II	0.3			
NpF2854g3	III	0.36	6.15	10	16
NpF4776g3	III	0.18	∼20	slow	20
NpR5113g2	II	0.17	16	16	
NpR6012g4	II	0.4			

models for describing the data is demonstrated by the excellent agreement between simulated kinetics and the observed data (Figures 3 and 4 and Figures S2−S6 in the SI). Multi-exponential excited-state decays in NpF2164g5, NpR5113g2, and NpF2854g3 are ascribed to the presence of two coexisting ground-state $^{152}P_r$ subpopulations, GS1 and GS2 (Figure 7), similar to the inhomogeneous target model constructed for the forward photodynamics of NpR6012g4.[37] Two ground-state subpopulations were also postulated for NpAF142g2, NpF2164g4, and NpR4776g3 (Figures S11 and S12 in the SI). NpF2164g6 required three ground-state subpopulations for a satisfactory description of the observed dynamics (Figures S3 and S12 in the SI), consistent with previous analysis of this protein.[31] In contrast, NpR1597g4 requires only one ground-state population (Figures S2, S11, and S12 in the SI) after weak thermal relaxation. Target analysis confirms the conservation of broadly similar behavior on the excited-state surface of all of the red/green CBCRs analyzed in these studies (Table 2, Figures 6 and 7, and Figures S11 and S12 in the SI). Upon photoexcitation, each subpopulation is excited to a $^{Hot}P_r$* state that subsequently decays into "relaxed" excited-state intermediates (ESI) on a relatively fast time scale of 1.5−6.5 ps without loss of the excited-state population. We have forced the SADS and decay constant of $^{Hot}P_r$* from each subpopulation in a given protein to be equal to simplify the modeling process. Relaxation of $^{Hot}P_r$* does not generate Lumi-R_f, in agreement with the sequential EADS analysis (Figure 6 and Figure S9 in the SI), and is characterized by red-shifting of the SE band (Figure 7 and Figure S12 of the SI). Such behavior has also been resolved in other CBCR and phytochrome systems.[42,52,53]

Class I CBCR NpF2164g5 does not generate Lumi-R_f; moreover, the relaxation of $^{Hot}P_r$* is unusually slow (6.5 ps, Figure 7 and Table 2). Both ESI populations decay back to their respective ground-state populations on 1.3 and 2 ns time scales (Figures 6 and 7). The $^{Hot}P_r$*, ESI1, and ESI2 SADS exhibit qualitatively similar features (black, red, and blue curves, respectively, in Figure 8A) with a pronounced negative amplitude on the long-wavelength side of the crossover region. The other class I sample, NpR1597g4, also exhibits unusually slow relaxation of $^{Hot}P_r$* (5.7 ps). In this case, global analysis could be used to calculate SADS-containing features of Lumi-R_f (Figure S12A in the SI) despite the absence of such features in the raw data (see above). However, fractional Lumi-R_f formation in NpR1597g4 was predicted to be notably lower than that in class II and class III proteins in this study (compare Figure S12A in the SI to Figure 7D and F and to Figures S12D, S12F, S12H, and S12J in the SI). This is consistent with the observed photoconversion of NpR1597g4 under continuous illumination, in contrast to that of NpF2164g5.[28]

In class II CBCRs NpR5113g2 and NpF2164g6, $^{Hot}P_r$* relaxation is much faster (0.3−2 ps) than in class I CBCRs NpF2164g5 and NpR1597g4. NpR5113g2 generates Lumi-R_f from both ESI1 and ESI2. ESI1 has an apparent lifetime of 153 ps with a $\Phi_{Lumi\text{-}Rf}$ value of 6.5%, and ESI2 has a 404 ps lifetime with a 19% $\Phi_{Lumi\text{-}Rf}$ value. Total $\Phi_{Lumi\text{-}Rf}$ is estimated to be 14% with initial occupancies of 39 and 61% for ESI1 and ESI2, respectively. The slower ESI2 population contributes 82% of the Lumi-R_f formation. The Lumi-R_f population decays on a 16 ns time scale without generating any discernible Meta-R_y, as evidenced by the slow decay of the 685 nm kinetic trace (Lumi-R_f) and concomitant decay of bleach (Figure 7B). As discussed

DOI: 10.1021/bi5012755
Biochemistry 2015, 54, 1028−1042

above, this decay could arise due to the formation of the starting $^{15Z}P_r$ ground state or due to the formation of a 15*E* intermediate that cannot be distinguished from the starting state. SADS of excited-state species $^{Hot}P_r$*, ESI1, and ESI2 are comparable in shape and amplitude. The other two class II CBCRs studied to date, NpF2164g6 and NpR6012g4, are both modeled with three ground-state subpopulations leading to three different excited-state intermediates. ESI1 and ESI2 are productive, whereas ESI3 is nonproductive (Table 2). In NpF2164g6, the SADS for nonproductive ESI3 for ground-state bleach is blue-shifted relative to those of $^{Hot}P_r$*, ESI1, and ESI2 (Figures S11 and S12C in the SI). This population thus has SADS similar to that of nonproductive, blue-shifted class I CBCR NpF2164g5 (Figure 8A). ESI1 and ESI2 both partition between the Lumi-R_f photoproduct and the $^{15Z}P_r$ starting state. Global analysis of class II CBCRs in this study is thus consistent with visual inspection of the raw data and sequential EADS analysis. Lumi-R_f formation is readily observed on an ultrafast time scale, but Meta-R_y formation is not.

Class III CBCRs such as NpF2854g3 also exhibit fast relaxation of $^{Hot}P_r$* (0.7−1.5 ps), two ground-state subpopulations, and two excited-state intermediates (Figures 6−8 and Figures S11 and S12 in the SI). Both ESI1 and ESI2 give rise to the Lumi-R_f photoproduct with varying time scales and efficiency (Tables 2 and 3). Overall, $\Phi_{Lumi\text{-}Rf}$ values range from 0.1 to 0.36, although the combination of slow Lumi-R_f formation and fast Meta-R_y formation in some cases of class III CBCRs implies that the $\Phi_{Lumi\text{-}Rf}$ values have larger uncertainty compared to those of other proteins in this study. In some cases, the kinetics of Lumi-R_f decay could not be adequately explained by Meta-R_y formation alone. Such cases were modeled as arising from the decay of Lumi-R_f back to the starting ground state (Table 3). As for NpR5113g2, this cannot be distinguished from the formation of a Meta-R_r species on this time scale. In NpF2854g3, Meta-R_y bleach has a greater amplitude than that of Lumi-R_f, suggesting that positive Lumi-R_f absorption overlaps negative GSB with the subsequent formation of blue-shifted Meta-R_y alleviating this overlap and restoring negative bleach amplitude. Other class III CBCRs show different patterns that are also consistent with overlap of Lumi-R_f and ground-state bleach, such as the shifting GSB peak wavelength in NpAF142g2 and NpF2164g4. Thus, class III CBCRs exhibit Meta-R_y formation that is much more rapid than that of class II proteins, while often exhibiting efficient primary photochemistry as shown by high values of $\Phi_{Lumi\text{-}Rf}$.

DISCUSSION

We have measured ultrafast forward ($^{15Z}P_r \rightarrow {}^{15E}P_g$) broadband TA signals for seven red/green CBCRs previously characterized only on a static time scale. Data for these seven proteins and new data for previously characterized NpF2164g6 were fit with global analysis routines, revealing three classes of red/green CBCRs on the basis of terminal photoproduct populations observed on an ultrafast time scale (<10 ns). The nine red/green CBCRs examined to date on the ultrafast time scale all exhibit typical red-absorbing $^{15Z}P_r$ dark states and include one example that fails to undergo photoconversion (NpF2164g5) and one example with an atypical red-shifted photoproduct (NpR1597g4). This cohort of CBCRs also exhibits great variation in the stability of the photoproduct with dark reversion rates ranging from 0.01 s^{-1} in NpF2164g6 to 4.4 × 10^{-6} s^{-1} in NpF2164g4. These proteins thus allow us to test whether previously characterized NpR6012g4 and NpF2164g6 provide a representative picture of primary photoisomerization in diverse red/green CBCRs and to ask whether the observed variation in static behavior is reflected in similar diversity on the ultrafast time scale. We find that there is considerable variation among red/green CBCRs on this time scale with large variations in their quantum yields, excited-state lifetimes, and primary photoproduct stabilities.

Excited-State Decay and Lumi-R_f Formation. The TA signals of class I NpF2164g5 and NpR1597g4 CBCRs did not exhibit obvious formation of Lumi-R_f primary photoproducts. Moreover, NpF2164g5 fails to undergo photoconversion under continuous illumination and exhibits high intrinsic fluorescence,[28] consistent with its long excited-state lifetime (Table 2). In contrast, NpR1597g4 does undergo photoconversion under continuous illumination and exhibits a red-shifted photoproduct, although the Lumi-R_f photoproduct could not be observed in the raw TA data for NpR1597g4 (Figure S2 in the SI). The results from global analysis of these two proteins are thus consistent with their static behavior,[28] implicating a very low but non-zero quantum yield for forward photoconversion of NpR1597g4 and essentially no photoproduct formation of NpF2164g5. These results also demonstrate that the lack of photoproduct formation on the longer time scale of NpF2164g5 is not due to efficient photoconversion followed by extremely rapid dark reversion. NpF2164g5 and NpR1597g4 exhibit distinct behaviors relative to class II and class III CBCRs immediately after excitation.

Eight of the nine red/green CBCRs studied to date initially produce a $^{Hot}P_r$* excited state upon excitation, including NpR1597g4 and NpF2164g5. Aside from these two cases, the $^{Hot}P_r$* of the others decays to yield P_r* on a time scale of 0.7−2 ps (Table 2). However, in these two proteins, the decay of $^{Hot}P_r$* is much slower (5−7 ps), and both proteins also exhibit slightly blue-shifted $^{15Z}P_r$ ground-state absorption relative to the other proteins in this study. It is thus possible that protein−chromophore interactions in these two proteins both produce this slight blue shift and constrain evolution of the initial excited-state packet, resulting in very slow evolution of the excited state both at the initial relaxation phase and at later decay time points of the excited-state intermediates. Alternately, the slow initial evolution of the excited state in these two proteins could reflect some process not seen in the other CBCRs, which diverts the excited-state population into a long-lived, less productive pathway. In this regard, it is interesting to note that the decay constants in productive CBCRs closest to the 5−7 ps time scale of NpF2164g5 and NpR1597g4 are for the decay of photochemically inactive ESI3 populations in NpR6012g4 and NpF2164g6 (4−5 ps, Table 2). Although the two cases describe different steps in the same process, they both involve nonproductive subpopulations and occur with very similar time constants. It is thus possible that similar changes in protein−chromophore interactions are at work in the nonproductive subpopulations of different red/green CBCRs.

In contrast to the class I CBCR samples, the class II and III proteins in this study produced readily detectable Lumi-R_f in varying yield (Table 1). Interestingly, no other protein exhibits the high quantum yield seen in NpR6012g4, although further pump-dump-probe experiments would be needed to resolve this question. The $\Phi_{Lumi\text{-}Rf}$ values estimated for the CBCRs in this study suggest that the SCID photoisomerization mechanism of NpR6012g4 is likely to be an exception rather than the rule. The productive CBCRs of classes II and III are

DOI: 10.1021/bi5012755
Biochemistry 2015, 54, 1028−1042

modeled with two to three ground-state subpopulations that each give rise to a distinct ESI, resulting in two to three excited-state intermediates. SADS for the individual ESI populations of each CBCR exhibit broadly similar features typically including residual ESA, and the negative band associated with GSB is red-shifted relative to the negative band in $^{Hot}P_r$*, consistent with contribution to the negative band from SE with a modest Stokes shift arising due to evolution of the excited-state population along the reaction coordinate. Decay of each ESI proceeds via rapid quenching (likely a conical intersection) of the excited-state population following excited-state barrier crossing; this nonadiabatic quenching is presumably responsible for most (if not all) of the branching between the Lumi-R_f photoproduct and the starting ground state.[37,51] One known exception is the SCID mechanism found in NpR6012g4, which involves reactive ground-state populations to increase the observed quantum yield of generating Lumi-R_f.[27]

The Lumi-R_f SADS of all class II and III CBCRs in this study have similar features with peak photoproduct absorptions at approximately 675 nm. Red/green CBCRs thus produce a red-shifted primary photoproduct similar to that seen in the forward reaction of cyanobacterial phytochrome Cph1, which has a very similar red-absorbing dark state but a far-red-absorbing photoproduct. The formation of a red-shifted primary photoproduct is also seen in other CBCRs, including green/red CBCR RcaE and inset-Cys CBCR NpF2164g3.[54,55] Although red-shifted primary photoproduct intermediates are the norm in CBCRs, not all such photoproducts are red-shifted; the formation of a blue-shifted Lumi-B_v primary photoproduct in the forward photoconversion of DXCF CBCR Tlr0924[52] thus seems exceptional. However, Tlr0924 is the only DXCF CBCR to have been examined on this time scale, so it is possible that this seemingly exceptional behavior will prove common among members of this particular subfamily.

Lumi-R_f Evolution. In NpR6012g4 and NpF2164g6, the Lumi-R_f photoproduct is stable on an ultrafast time scale with no apparent decay (Table 3). The other class II protein, NpR5113g2, exhibits slow decay of Lumi-R_f without detectable formation of the Meta-R_y intermediate observed in class III proteins (see below). Such behavior could arise from the decay of Lumi-R_f back into the initial $^{15Z}P_r$ ground state, implying nonunity yield of stable photoproduct $^{15E}P_g$ from Lumi-R_f. Alternately, it could arise from formation of a productive Meta-R_r species that is red-shifted relative to the Meta-R_y species seen in class III proteins with a positive absorption that overlaps the negative GSB band. Our TA data do not allow us to distinguish between these hypotheses, and such a Meta-R_r species has not yet been resolved in either our work or slower flash photolysis studies of AnPixJ.[30] We have therefore modeled Lumi-R_f decay in NpR5113g2 to result in the regeneration of $^{15Z}P_r$. Examination of NpR5113g2 and other red/green CBCRs using time-resolved vibrational techniques will aid in unraveling Lumi-R_f evolution in this protein.

Unlike class II proteins, class III proteins exhibit detectable formation of Meta-R_y on an ultrafast time scale. This blue-shifted intermediate has not been reported in the forward dynamics of phytochromes,[56] demonstrating that forward photoconversion of red/far-red phytochromes and red/green CBCRs diverge well before final photoproduct formation. Meta-R_y is spectrally similar to the $R2_{610}$ intermediate observed in the forward dynamics of AnPixJg2 by Fukushima et al., although this species formed on a much slower time scale (>50 ns).[30] To gain more information about subsequent events in red/green CBCRs, we also compared transient spectra at 1 ms to Lumi-R_f and Meta-R_y SADS (Figure 9). As expected given

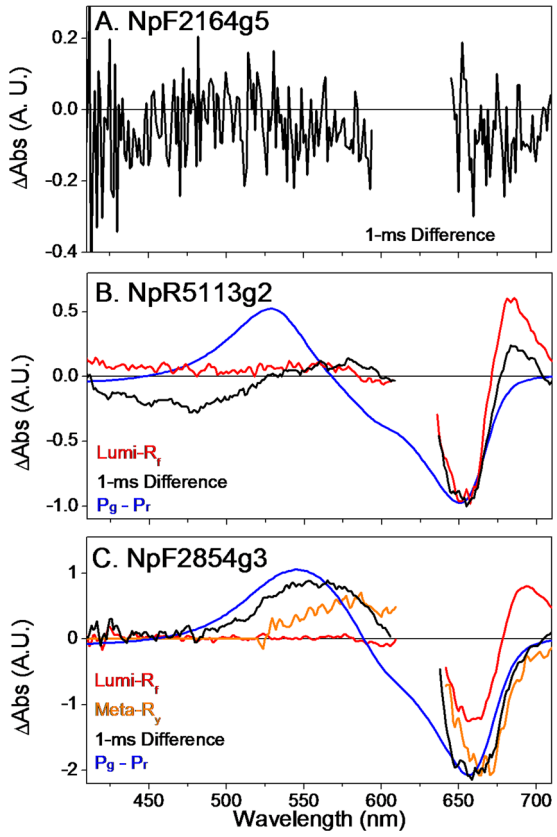

Figure 9. Comparison of the $^{15E}P_g$–$^{15Z}P_r$ difference spectrum, the 1 ms difference spectrum, and the Lumi-R_f and Meta-R_y spectra (blue, black, red, and orange curves, respectively) for (A) NpF2164g5, (B) NpR5113g2, and (C) NpF2854g3. The $^{15E}P_g$–$^{15Z}P_r$ difference spectra are constructed from their respective ground-state spectra normalized at the 280 nm peak. Photoinactive NpF2164g5 (A) has only the 1 ms difference spectrum shown here due to its lack of $^{15E}P_g$ generation. The 1 ms difference spectra are smoothed for clarity.

the lack of Lumi-R_f formation in NpF2164g5, the 1 ms transient spectrum for this protein shows no change relative to the ground state (Figure 9A). In NpR5113g2, Lumi-R_f absorption persists even at 1 ms, demonstrating that Meta-R_y formation in this protein is extremely slow. Contrastingly, the 1 ms spectrum in NpF2854g3 reveals further blue-shifting of the photoproduct peak without final formation of the stable $^{15E}P_g$ photoproduct (Figure 9C). Although a detailed analysis of longer time points is necessary, it is thus clear that kinetic differences on the ultrafast time scale can persist at later stages of photoconversion.

Protein–Chromophore Interactions and Ultrafast Photodynamics. Our study provides a unique opportunity to compare ground-state and ultrafast properties for a group of proteins with largely conserved protein–chromophore interactions (Figure S13 in the SI). There is an overall correlation between photochemical quantum yield and rapid excited-state decay (Figure 10A). This trend is not surprising as similar behavior has been reported in other photoreceptor systems.[31,37,51,52,54,55] Interestingly, $\Phi_{Lumi\text{-}Rf}$ is also roughly correlated with the decay constant for $^{Hot}P_r$* (Figure 10B). This could indicate that the initial evolution of the excited

DOI: 10.1021/bi5012755
Biochemistry 2015, 54, 1028–1042

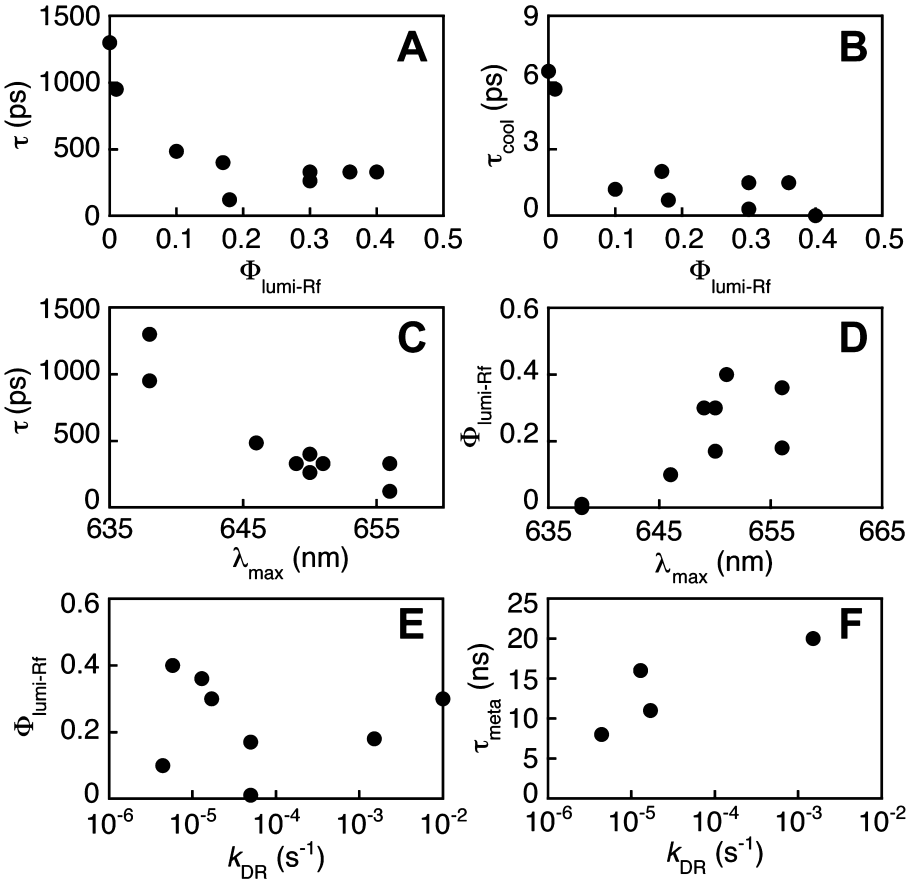

Figure 10. Correlation plots for red/green CBCRs. (A) Correlation between $\Phi_{Lumi-Rf}$ and the slowest excited-state decay constant. (B) Correlation between $\Phi_{Lumi-Rf}$ and the time constant for relaxation of $^{Hot}P_r$*. (C) Correlation between the peak wavelength for $^{15Z}P_r$ ground-state absorption and the slowest excited-state decay constant. (D) Correlation between peak wavelength and $\Phi_{Lumi-Rf}$. (E) Lack of correlation between dark reversion rate (red/green) and $\Phi_{Lumi-Rf}$. (F) Correlation between dark reversion rate and estimated time constant for Meta-R_y formation.

wavepacket determines $\Phi_{Lumi-Rf}$; however, the correlation is not very tight, so it seems unlikely that the observed differences in $\Phi_{Lumi-Rf}$ values for proteins in this study arise due to excited-state bifurcation rather than ground-state heterogeneity. There is also a rough correlation between the excited-state lifetime, $\Phi_{Lumi-Rf}$, and $^{15Z}P_r$ peak wavelength (Figure 10C and D). CBCRs with red-shifted peak wavelengths exhibit faster excited-state decay and higher $\Phi_{Lumi-Rf}$ values. A similar phenomenon has been reported in Cph1, in which a blue-shifted P_r subpopulation exhibits slower excited-state dynamics, higher intrinsic fluorescence, and lower photochemical quantum yield.[57,58] However, the lower quantum yield but red-shifted P_r of Cph1 relative to red/green CBCRs demonstrates that these are two examples of similar phenomena rather than a single trend. Taken together, these observations indicate that very modest changes in chromophore positioning within the pocket have significant effects on photoconversion efficiency.

The CBCRs in this study also exhibit great variation in the rate of dark reversion. That the variation does not correlate with $\Phi_{Lumi-Rf}$ (Figure 10E) is unsurprising given that dark reversion is a property of the $^{15E}P_g$ photoproduct state and $\Phi_{Lumi-Rf}$ is a property of P_r* in red/green CBCRs. However, there is an apparent correlation between the rate of dark reversion and the time constant for Meta-R_y formation in cases in which Meta-R_y formation is resolved (Figure 10F). Both of these processes proceed in the absence of light and are apparently dictated by protein−chromophore interactions, so this rough correlation may indicate that protein motions favoring dark reversion (i.e., spontaneous reverse conversion) disfavor secondary dynamics of forward photoconversion. However, CBCRs in which Meta-R_y formation was not resolved include NpF2164g6 and NpR6012g4.

We are currently not able to identify specific protein−chromophore interactions that are responsible for the observed variation in ultrafast photodynamics of the proteins in this study. Class I CBCR NpF2164g5 has several substitutions at conserved positions, but introducing similar substitutions into NpR6012g4 did not ablate photoconversion.[39] Similarly, NpR5113g2 has a Phe residue in place of the conserved Tyr on the first β strand of the CBCR GAF domain. Substitutions for this Tyr produce profound effects on Cph1, but similar substitutions have little effect on NpR6012g4.[39,59,60] Moreover, the same substitution of Phe for Tyr is also found in NpR4776g3, demonstrating that there is no apparent correlation between the presence of this residue and a range of ultrafast properties, including the decay kinetics for P_r* and the stability of Lumi-R_f (Tables 2 and 3). Interestingly, NpR5113g2 and NpR1597g4 lack a Trp residue that is conserved in red/green CBCRs.[39] Both of these proteins have $\Phi_{Lumi-Rf}$ values that are relatively low compared to those of other proteins in this study (Table 1). It is thus possible that this Trp residue can aid in positioning the chromophore for more efficient photoconversion, consistent with the formation of blue-shifted 15*Z* side populations in NpR6012g4 variants

DOI: 10.1021/bi5012755
Biochemistry 2015, 54, 1028−1042

that have aliphatic amino acids in place of this residue.[39] Similarly, NpAF142g2 and NpF2854g3 have a small insertion in the second β strand of the GAF domain and also have $\Phi_{\text{Lumi-Rf}}$ values that are relatively high compared to those of other proteins in this study (Table 1). A conserved Phe residue on β2 contacts the chromophore in the AnPixJ crystal structure and is critical for photoproduct tuning in both NpR6012g4 and NpR5113g2.[39] The insertion found in NpF2854g3 and NpAF142g2 may change the steric packing in this region in the $^{15Z}P_r$ dark state, resulting in a less crowded chromophore environment that faciliates a more rapid evolution. A more flexible chromophore binding pocket in such proteins may also explain why these proteins are two of the four class III CBCRs in this study, because the extra flexibility of the dark-state pocket may also facilitate rapid Meta-R_y formation.

Despite these detail differences, our study allows several conclusions to be drawn about forward photoconversion in red/green CBCRs. Almost all such proteins exhibit the formation of Lumi-R_f photoproducts with very similar spectral properties, albeit with varying $\Phi_{\text{Lumi-Rf}}$ values. Lumi-R_f subsequently evolves to give rise to Meta-R_y, although the rate of this process varies considerably. Subsequent evolution of Meta-R_y has not been addressed in this study, but the 1 ms transient spectrum of NpF2854g3 (Figure 9C) and flash photolysis studies of AnPixJ[30] are consistent with direct conversion of Meta-R_y to $^{15E}P_g$ on a millisecond time scale. Red/green CBCRs thus seem to have a conserved mechanism for forward photoconversion with two intermediates. It will be interesting to see whether this mechanism is also found in the NpR3784 family of red/green BCRs, which have a similar red/green photocycle due to distinct protein−chromophore interactions,[61] and whether similar conservation is found in reverse photoconversion for the proteins in this study.

■ ASSOCIATED CONTENT

Supporting Information

Absorption spectra, additional transient signals, quantum yield analyses, sequential EADS analyses, additional target model analyses, and a stereogram of the chromophore binding pocket. This material is available free of charge via the Internet at http://pubs.acs.org.

■ AUTHOR INFORMATION

Corresponding Author

*E-mail: dlarsen@ucdavis.edu. Tel: (530) 754-9075.

Funding

This work was supported by a grant from the Chemical Sciences, Geosciences, and Biosciences Division, Office of Basic Energy Sciences, Office of Science, United States Department of Energy (DOE DE-FG02-09ER16117), to both J.C.L. and D.S.L.

Notes

The authors declare no competing financial interest.

■ ACKNOWLEDGMENTS

Dr. Mikas Vengris (Light Conversion Ltd.) is acknowledged for the donation of the global and target analysis software package.

■ ABBREVIATIONS

CBCR, cyanobacteriochrome; CBD, chitin binding domain; CD, circular dichroism; EADS, evolution-associated difference spectrum; SADS, species-associated difference spectra; ESI, excited-state intermediate; ESA, excited-state absorption; SE, stimulated emission; GAF, domain name derived from cGMP phosphodiesterase/adenylyl cyclase/FhlA; GSA, ground-state absorbance; PAS, Per-ARNT-Sim; PΦB, phytochromobilin; PCB, phycocyanobilin; P_r, red-absorbing ground state of red/far-red phytochromes; P_{fr}, far-red-absorbing photoproduct state of red/far-red phytochromes; $^{15Z}P_r$, red-absorbing ground state of red/green CBCRs; $^{15E}P_g$, green-absorbing photoproduct state of red/green CBCRs; P_g*, excited-state population(s) derived from photoexcitation of P_g or $^{15E}P_g$; PYP, photoactive yellow protein; Φ, total photocycle quantum yield; $\Phi_{\text{Lumi-Rf}}$, quantum yield of generating Lumi-R_f; Φ_{meta}, quantum yield of generating Meta-R; Φ_f, fluorescence quantum yield

■ REFERENCES

(1) Shu, X. K., Royant, A., Lin, M. Z., Aguilera, T. A., Lev-Ram, V., Steinbach, P. A., and Tsien, R. Y. (2009) Mammalian expression of infrared fluorescent proteins engineered from a bacterial phytochrome. *Science 324*, 804−807.

(2) Moglich, A., and Moffat, K. (2010) Engineered photoreceptors as novel optogenetic tools. *Photochem. Photobiol. Sci. 9*, 1286−1300.

(3) Drepper, T., Krauss, U., Berstenhorst, S. M. Z., Pietruszka, J., and Jaeger, K. E. (2011) Lights on and action! Controlling microbial gene expression by light. *Appl. Microbiol. Biotechnol. 90*, 23−40.

(4) Van der Horst, M. A., and Hellingwerf, K. J. (2004) Photoreceptor proteins, "star actors of modern times": A review of the functional dynamics in the structure of representative members of six different photoreceptor families. *Acc. Chem. Res. 37*, 13−20.

(5) Rockwell, N. C., and Lagarias, J. C. (2010) A brief history of phytochromes. *ChemPhysChem 11*, 1172−1180.

(6) Narikawa, R., Fukushima, Y., Ishizuka, T., Itoh, S., and Ikeuchi, M. (2008) A novel photoactive GAF domain of cyanobacteriochrome AnPixJ that shows reversible green/red photoconversion. *J. Mol. Biol. 380*, 844−855.

(7) Briggs, W. R., and Spudich, J. L., Eds. (2005) *Handbook of Photosensory Receptors*, Wiley-VCH, Weinheim, Germany.

(8) Moglich, A., Yang, X. J., Ayers, R. A., and Moffat, K. (2010) Structure and function of plant photoreceptors. *Annu. Rev. Plant Biol. 61*, 21−47.

(9) Hughes, J. (2013) Phytochrome cytoplasmic signaling. *Annu. Rev. Plant Biol. 64*, 377−402.

(10) Franklin, K. A., and Quail, P. H. (2010) Phytochrome functions in *Arabidopsis* development. *J. Exp. Bot. 61*, 11−24.

(11) Quail, P. H. (2002) Phytochrome photosensory signalling networks. *Nat. Rev. Mol. Cell Biol. 3*, 85−93.

(12) Auldridge, M. E., and Forest, K. T. (2011) Bacterial phytochromes: more than meets the light. *Crit. Rev. Biochem. Mol. Biol. 46*, 67−88.

(13) Rockwell, N. C., Duanmu, D., Martin, S. S., Bachy, C., Price, D. C., Bhattacharya, D., Worden, A. Z., and Lagarias, J. C. (2014) Eukaryotic algal phytochromes span the visible spectrum. *Proc. Natl. Acad. Sci. U.S.A. 111*, 3871−3876.

(14) Blumenstein, A., Vienken, K., Tasler, R., Purschwitz, J., Veith, D., Frankenberg-Dinkel, N., and Fischer, R. (2005) The *Aspergillus nidulans* phytochrome FphA represses sexual development in red light. *Curr. Biol. 15*, 1833−1838.

(15) Brandt, S., von Stetten, D., Gunther, M., Hildebrandt, P., and Frankenberg-Dinkel, N. (2008) The fungal phytochrome FphA from *Aspergillus nidulans*. *J. Biol. Chem. 283*, 34605−34614.

(16) Rockwell, N. C., Su, Y. S., and Lagarias, J. C. (2006) Phytochrome structure and signaling mechanisms. *Annu. Rev. Plant Biol. 57*, 837−858.

(17) Song, C., Psakis, G., Lang, C., Mailliet, J., Gartner, W., Hughes, J., and Matysik, J. (2011) Two ground state isoforms and a chromophore D-ring photoflip triggering extensive intramolecular changes in a canonical phytochrome. *Proc. Natl. Acad. Sci. U.S.A. 108*, 3842−3847.

DOI: 10.1021/bi5012755
Biochemistry 2015, 54, 1028−1042

(18) Yang, X., Ren, Z., Kuk, J., and Moffat, K. (2011) Temperature-scan cryocrystallography reveals reaction intermediates in bacteriophytochrome. *Nature 479*, 428−432.
(19) Song, C., Psakis, G., Kopycki, J., Lang, C., Matysik, J., and Hughes, J. (2014) The D-ring, not the A-ring, rotates in *Synechococcus* OS-B′ phytochrome. *J. Biol. Chem. 289*, 2552−2562.
(20) Wagner, J. R., Brunzelle, J. S., Forest, K. T., and Vierstra, R. D. (2005) A light-sensing knot revealed by the structure of the chromophore-binding domain of phytochrome. *Nature 438*, 325−331.
(21) Ulijasz, A. T., Cornilescu, G., von Stetten, D., Kaminski, S., Mroginski, M. A., Zhang, J. R., Bhaya, D., Hildebrandt, P., and Vierstra, R. D. (2008) Characterization of two thermostable cyanobacterial phytochromes reveals global movements in the chromophore-binding domain during photoconversion. *J. Biol. Chem. 283*, 21251−21266.
(22) Gan, F., Zhang, S., Rockwell, N. C., Martin, S. S., Lagarias, J. C., and Bryant, D. A. (2014) Extensive remodeling of a cyanobacterial photosynthetic apparatus in far-red light. *Science 345*, 1312−1317.
(23) Ikeuchi, M., and Ishizuka, T. (2008) Cyanobacteriochromes: a new superfamily of tetrapyrrole-binding photoreceptors in cyanobacteria. *Photochem. Photobiol. Sci. 7*, 1159−1167.
(24) Enomoto, G., Nomura, R., Shimada, T., Win, N. N., Narikawa, R., and Ikeuchi, M. (2014) Cyanobacteriochrome SesA is a diguanylate cyclase that induces cell aggregation in *Thermosynechococcus*. *J. Biol. Chem. 289*, 24801−24809.
(25) Rockwell, N. C., Martin, S. S., Feoktistova, K., and Lagarias, J. C. (2011) Diverse two-cysteine photocycles in phytochromes and cyanobacteriochromes. *Proc. Natl. Acad. Sci. U.S.A. 108*, 11854−11859.
(26) Rockwell, N. C., Martin, S. S., Gulevich, A. G., and Lagarias, J. C. (2012) Phycoviolobilin formation and spectral tuning in the DXCF cyanobacteriochrome subfamily. *Biochemistry 51*, 1449−1463.
(27) Kim, P. W., Freer, L. H., Rockwell, N. C., Martin, S. S., Lagarias, J. C., and Larsen, D. S. (2012) Second-chance forward isomerization dynamics of the red/green cyanobacteriochrome NpR6012g4 from *Nostoc punctiforme*. *J. Am. Chem. Soc. 134*, 130−133.
(28) Rockwell, N. C., Martin, S. S., and Lagarias, J. C. (2012) Red/green cyanobacteriochromes: sensors of color and power. *Biochemistry 51*, 9667−9677.
(29) Narikawa, R., Ishizuka, T., Muraki, N., Shiba, T., Kurisu, G., and Ikeuchi, M. (2013) Structures of cyanobacteriochromes from phototaxis regulators AnPixJ and TePixJ reveal general and specific photoconversion mechanism. *Proc. Natl. Acad. Sci. U.S.A. 110*, 918−923.
(30) Fukushima, Y., Iwaki, M., Narikawa, R., Ikeuchi, M., Tomita, Y., and Itoh, S. (2011) Photoconversion mechanism of a green/red photosensory cyanobacteriochrome AnPixJ: time-resolved optical spectroscopy and FTIR analysis of the AnPixJ-GAF2 domain. *Biochemistry 50*, 6328−6339.
(31) Chang, C. W., Gottlieb, S. M., Kim, P. W., Rockwell, N. C., Lagarias, J. C., and Larsen, D. S. (2013) Reactive ground-state pathways are not ubiquitous in red/green cyanobacteriochromes. *J. Phys. Chem. B 117*, 11229−11238.
(32) Gambetta, G. A., and Lagarias, J. C. (2001) Genetic engineering of phytochrome biosynthesis in bacteria. *Proc. Natl. Acad. Sci. U.S.A. 98*, 10566−10571.
(33) Hirose, Y., Rockwell, N. C., Nishiyama, K., Narikawa, R., Ukaji, Y., Inomata, K., Lagarias, J. C., and Ikeuchi, M. (2013) Green/red cyanobacteriochromes regulate complementary chromatic acclimation via a protochromic photocycle. *Proc. Natl. Acad. Sci. U.S.A. 110*, 4974−4979.
(34) Miroux, B., and Walker, J. E. (1996) Over-production of proteins in *Escherichia coli*: mutant hosts that allow synthesis of some membrane proteins and globular proteins at high levels. *J. Mol. Biol. 260*, 289−298.
(35) Mukougawa, K., Kanamoto, H., Kobayashi, T., Yokota, A., and Kohchi, T. (2006) Metabolic engineering to produce phytochromes with phytochromobilin, phycocyanobilin, or phycoerythrobilin chromophore in *Escherichia coli*. *FEBS Lett. 580*, 1333−1338.
(36) Carroll, E. C., Compton, O. C., Madsen, D., Osterloh, F. E., and Larsen, D. S. (2008) Ultrafast carrier dynamics in exfoliated and functionalized calcium niobate nanosheets in water and methanol. *J. Phys. Chem. C 112*, 2394−2403.
(37) Kim, P. W., Freer, L. H., Rockwell, N. C., Martin, S. S., Lagarias, J. C., and Larsen, D. S. (2012) Femtosecond photodynamics of the red/green cyanobacteriochrome NpR6012g4 from *Nostoc punctiforme*. 1. Forward dynamics. *Biochemistry 51*, 608−618.
(38) Spillane, K. M., Dasgupta, J., Lagarias, J. C., and Mathies, R. A. (2009) Homogeneity of phytochrome Cph1 vibronic absorption revealed by resonance Raman intensity analysis. *J. Am. Chem. Soc. 131*, 13946−13948.
(39) Rockwell, N. C., Martin, S. S., Gulevich, A. G., and Lagarias, J. C. (2014) Conserved phenylalanine residues are required for blue-shifting of cyanobacteriochrome photoproducts. *Biochemistry 53*, 3118−3130.
(40) Gottlieb, S. M., Corley, S. C., Madsen, D., and Larsen, D. S. (2012) Note: a flexible light emitting diode-based broadband transient-absorption spectrometer. *Rev. Sci. Instrum. 83*, 056107.
(41) Fitzpatrick, A. E., Lincoln, C. N., van Wilderen, L. J., and van Thor, J. J. (2012) Pump-dump-probe and pump-repump-probe ultrafast spectroscopy resolves cross section of an early ground state intermediate and stimulated emission in the photoreactions of the Pr ground state of the cyanobacterial phytochrome Cph1. *J. Phys. Chem. B 116*, 1077−1088.
(42) Kim, P. W., Pan, J., Rockwell, N. C., Chang, C.-W., Taylor, K. C., Lagarias, J. C., and Larsen, D. S. (2012) Ultrafast E to Z photoisomerization dynamics of the Cph1 phytochrome. *Chem. Phys. Lett. 549*, 86−92.
(43) Toh, K. C., Stojkovic, E. A., van Stokkum, I. H. M., Moffat, K., and Kennis, J. T. M. (2010) Proton-transfer and hydrogen-bond interactions determine fluorescence quantum yield and photochemical efficiency of bacteriophytochrome. *Proc. Natl. Acad. Sci. U.S.A. 107*, 9170−9175.
(44) Muller, M. G., Lindner, I., Martin, I., Gartner, W., and Holzwarth, A. R. (2008) Femtosecond kinetics of photoconversion of the higher plant photoreceptor phytochrome carrying native and modified chromophores. *Biophys. J. 94*, 4370−4382.
(45) Heyne, K., Herbst, J., Stehlik, D., Esteban, B., Lamparter, T., Hughes, J., and Diller, R. (2002) Ultrafast dynamics of phytochrome from the cyanobacterium *Synechocystis*, reconstituted with phycocyanobilin and phycoerythrobilin. *Biophys. J. 82*, 1004−1016.
(46) Bischoff, M., Hermann, G., Rentsch, S., and Strehlow, D. (2001) First steps in the phytochrome phototransformation: a comparative femtosecond study on the forward (Pr → Pfr) and back reaction (Pfr → Pr). *Biochemistry 40*, 181−186.
(47) Rentsch, S., Hermann, G., Bischoff, M., Strehlow, D., and Rentsch, M. (1997) Femtosecond spectroscopic studies on the red light-absorbing form of oat phytochrome and 2,3-dihydrobiliverdin. *Photochem. Photobiol. 66*, 585−590.
(48) Lamparter, T., Esteban, B., and Hughes, J. (2001) Phytochrome Cph1 from the cyanobacterium *Synechocystis* PCC6803: purification, assembly, and quaternary structure. *Eur. J. Biochem. 268*, 4720−4730.
(49) van Stokkum, I. H. M., Larsen, D. S., and van Grondelle, R. (2004) Global and target analysis of time-resolved spectra. *Biochim. Biophys. Acta, Bioenerg. 1657*, 82−104.
(50) Holzwarth, A. R. (1996) Data analysis of time-resolved measurements. In *Biophysical Techniques in Photosynthesis* (Amesz, J., and Hoff, A. J., Eds.) pp 75−92, Springer, Dordrecht, The Netherlands.
(51) Kim, P. W., Freer, L. H., Rockwell, N. C., Martin, S. S., Lagarias, J. C., and Larsen, D. S. (2012) Femtosecond photodynamics of the red/green cyanobacteriochrome NpR6012g4 from *Nostoc punctiforme*. 2. Reverse dynamics. *Biochemistry 51*, 619−630.
(52) Freer, L. H., Kim, P. W., Corley, S. C., Rockwell, N. C., Zhao, L., Thibert, A. J., Lagarias, J. C., and Larsen, D. S. (2012) Chemical inhomogeneity in the ultrafast dynamics of the DXCF cyanobacteriochrome Tlr0924. *J. Phys. Chem. B 116*, 10571−10581.
(53) Holzwarth, A. R., Wendler, J., Schaffner, K., Sundstrom, V., Sandstrom, A., and Gillbro, T. (1983) Phytochrome models 0.8. Picosecond kinetics of excited-state relaxation in biliverdin dimethyl ester. *Isr. J. Chem. 23*, 223−231.

DOI: 10.1021/bi5012755
Biochemistry 2015, 54, 1028−1042

(54) Gottlieb, S. M., Kim, P. W., Rockwell, N. C., Hirose, Y., Ikeuchi, M., Lagarias, J. C., and Larsen, D. S. (2013) Primary photodynamics of the green/red-absorbing photoswitching regulator of the chromatic adaptation E domain from *Fremyella diplosiphon*. *Biochemistry 52*, 8198−8208.
(55) Gottlieb, S. M., Kim, P. W., Corley, S. C., Madsen, D., Hanke, S. J., Chang, C. W., Rockwell, N. C., Martin, S. S., Lagarias, J. C., and Larsen, D. S. (2014) Primary and secondary photodynamics of the violet/orange dual-cysteine NpF2164g3 cyanobacteriochrome domain from *Nostoc punctiforme*. *Biochemistry 53*, 1029−1040.
(56) Zhang, C. F., Farrens, D. L., Bjorling, S. C., Song, P. S., and Kliger, D. S. (1992) Time-resolved absorption studies of native etiolated oat phytochrome. *J. Am. Chem. Soc. 114*, 4569−4580.
(57) Kim, P. W., Rockwell, N. C., Martin, S. S., Lagarias, J. C., and Larsen, D. S. (2014) Heterogeneous photodynamics of the P_{fr} state in the cyanobacterial phytochrome Cph1. *Biochemistry 53*, 4601−4611.
(58) Kim, P. W., Rockwell, N. C., Freer, L. H., Chang, C.-W., Martin, S. S., Lagarias, J. C., and Larsen, D. S. (2013) Unraveling the primary isomerization dynamics in the Cph1 cyanobacterial phytochrome with multipulse manipulations. *J. Phys. Chem. Lett. 4*, 2605−2609.
(59) Fischer, A. J., and Lagarias, J. C. (2004) Harnessing phytochrome's glowing potential. *Proc. Natl. Acad. Sci. U.S.A. 101*, 17334−17339.
(60) Fischer, A. J., Rockwell, N. C., Jang, A. Y., Ernst, L. A., Waggoner, A. S., Duan, Y., Lei, H. X., and Lagarias, J. C. (2005) Multiple roles of a conserved GAF domain tyrosine residue in cyanobacterial and plant phytochromes. *Biochemistry 44*, 15203−15215.
(61) Rockwell, N. C., Martin, S. S., Gan, F., Bryant, D. A., and Lagarias, J. C. (2014) NpR3784 is the prototype for a group of red/green cyanobacteriochromes using alternative Phe residues for photoproduct tuning. *Photochem. Photobiol. Sci.*, DOI: 10.1039/C4PP00336E.

DOI: 10.1021/bi5012755
Biochemistry 2015, 54, 1028−1042